# High–Reynolds Number Wall Turbulence

Alexander J. Smits,[1] Beverley J. McKeon,[2] and Ivan Marusic[3]

[1]Department of Mechanical and Aerospace Engineering, Princeton University, Princeton, New Jersey 08544; email: asmits@princeton.edu

[2]Graduate Aerospace Laboratories, California Institute of Technology, Pasadena, California 91125; email: mckeon@caltech.edu

[3]Department of Mechanical Engineering, University of Melbourne, VIC 3010 Melbourne, Australia; email: imarusic@unimelb.edu.au

Annu. Rev. Fluid Mech. 2011. 43:353–75

First published online as a Review in Advance on September 14, 2010

The *Annual Review of Fluid Mechanics* is online at fluid.annualreviews.org

This article's doi: 10.1146/annurev-fluid-122109-160753



0066-4189/11/0115-0353$20.00

## Keywords

boundary layers, channel flow, pipe flow, coherent motions, turbulence structure

## Abstract

We review wall-bounded turbulent flows, particularly high–Reynolds number, zero–pressure gradient boundary layers, and fully developed pipe and channel flows. It is apparent that the approach to an asymptotically high–Reynolds number state is slow, but at a sufficiently high Reynolds number the log law remains a fundamental part of the mean flow description. With regard to the coherent motions, very-large-scale motions or superstructures exist at all Reynolds numbers, but they become increasingly important with Reynolds number in terms of their energy content and their interaction with the smaller scales near the wall. There is accumulating evidence that certain features are flow specific, such as the constants in the log law and the behavior of the very large scales and their interaction with the large scales (consisting of vortex packets). Moreover, the refined attached-eddy hypothesis continues to provide an important theoretical framework for the structure of wall-bounded turbulent flows.

## 1. INTRODUCTION

We review Reynolds number effects on wall-bounded turbulent flows, with a particular emphasis on high–Reynolds number flows. The subject of wall-bounded turbulence has a distinguished history, and it is not surprising that it has been the topic of a number of reviews, notably Cantwell (1981) and Robinson (1991) on the structure of the organized motions and Panton (2001) on the mechanisms by which wall turbulence sustains itself. Detailed discussions on the turbulence statistics are given in the reviews by Gad-el Hak & Bandyopadhyay (1994), Fernholz & Finley (1996), and Klewicki (2010). A number of collections specializing in this area have also appeared relatively recently, including Walker (1991), Panton (1997), Donnelly & Sreenivasan (1998), Smits (2004), and McKeon (2007). We also note Marusic et al. (2010c), who summarized the outcomes of a series of workshops on the effects of Reynolds number held between 2003 and 2008.

It is an opportune time to build on this work, and review our current understanding of high–Reynolds number turbulent flows. Barenblatt (1993) and Barenblatt et al. (1997) triggered one of the major controversies in recent times regarding wall-bounded turbulent flows when they suggested that power laws provide a more accurate description for the mean velocity profile than the classical wall/wake formulation first advanced by Coles (1956) (see the sidebar Law of the Wall/Law of the Wake). The controversy had the fortunate effect of stimulating a great deal of new work. Innovative experiments have proliferated with the availability of new laboratory facilities capable of generating high–Reynolds number flows, including the Princeton Superpipe (Zagarola & Smits 1998), the Minimum Turbulence Level wind tunnel at KTH (Österlund 1999), the National Diagnostic Facility at the Illinois Institute of Technology (Hites 1997), and the High Reynolds Number Boundary Layer Wind Tunnel at Melbourne University (Nickels et al. 2007). Since about 1997, the Surface Layer Turbulence and Environmental Science Test facility in Utah (Metzger 2002) has provided high-quality data in the atmospheric boundary layer (ABL), which has been invaluable for studying the behavior at Reynolds numbers one or two orders of magnitude larger than what is possible in the laboratory. Also, new scaling arguments have been advanced by George & Castillo (1997), DeGraaff & Eaton (2000), Wei et al. (2005), Monkewitz et al. (2007), and Panton (2007), for example, which have led to much debate within the community. In addition, direct numerical simulations (DNS) of channel flows up to $Re_\tau = 2{,}003$ ($Re_b \approx 90 \times 10^3$) are now available (Hoyas & Jiménez 2006), compared with 180 in 1987 (Kim et al. 1987), and recent work by Schlatter et al. (2010) has pushed DNS of spatially developing boundary layers to $Re_\theta = 4{,}300$ ($Re_\tau \approx 1{,}300$). Here, $Re_\tau = hu_\tau/\nu$, where $h$ is the half-channel width, $u_\tau$ is the friction velocity, and $\nu$ is the fluid kinematic viscosity. For pipes and boundary layers, we use the pipe radius $R$ or the boundary-layer thickness $\delta$ instead of $h$ in the definition of $Re_\tau$. Also, $Re_\theta = \theta U_e/\nu$, where $\theta$

### LAW OF THE WALL/LAW OF THE WAKE

In Coles's (1956) description, the velocity profile outside the viscous-dominated near-wall region is described as the sum of a logarithmic part and a wake component, so that the variation of the mean velocity $U$ with distance from the wall $y$ is described by

$$\frac{U}{u_\tau} = \frac{1}{\kappa}\ln\frac{yu_\tau}{\nu} + B + \frac{2\Pi}{\kappa}W\left(\frac{y}{\delta}\right),$$

where $u_\tau$ is the friction velocity, $\nu$ is the fluid kinematic viscosity, $\delta$ is the boundary-layer thickness, $W$ is the wake function, and $\Pi$ is the wake factor. Here, $B$ and $\kappa$ are constants, called the additive constant and von Kármán's constant, respectively.

is the momentum thickness and $U_e$ is the free-stream velocity, and $Re_D = 2R\langle U \rangle/\nu$, where $\langle U \rangle$ is the area-averaged or bulk velocity.

As shown below, these investigations have provided fresh insights into the high–Reynolds number behavior of the mean flow, the scaling of the turbulence statistics, and the evolution of the spectra, and they have uncovered a new class of organized motions that are many times larger than the characteristic dimension of the flow, as well as revealed previously unsuspected connections among the different types of organized motions. Most interesting, perhaps, is the growing appreciation that pipe, channel, and boundary-layer flows may behave differently in important aspects, such as the slope of the logarithmic velocity variation, the scaling of the near-wall turbulence, and the nature of the largest scales.

Here, we confine our discussion to canonical incompressible flows: zero–pressure gradient boundary layers and fully developed pipe and channel flows. We begin with a review of what we currently understand by the description of a high Reynolds number, followed by a description of new aspects of the mean flow behavior and the current view of the structure of wall-bounded turbulence and its relation to the scaling of the turbulence statistics. We then summarize the aspects of turbulent flow that do not appear to be specific to or dependent on Reynolds number, examine the continued utility of the attached-eddy hypothesis, and attempt to delineate the prospects for future progress as new facilities, computers, and diagnostic tools become available.



## 2. HIGH REYNOLDS NUMBER

What are high–Reynolds number flows, and how are they different from low–Reynolds number flows? These are important questions because the vast majority of previous experiments in wall turbulence, and unavoidably all DNS, have been performed at low to moderate Reynolds numbers. In many cases, the focus on low Reynolds number has been deliberate as experimentally this provides a physically thick viscous near-wall region, which makes it easier to study the coherent near-wall streaky motions. A number of proposed drag-reduction strategies are based on the manipulation of these near-wall events, and many theories are based on the premise that the near-wall structures propagate and self-sustain without the need for an external trigger [e.g., see the review by Panton (2001)]. Such autonomous views are emphasized in the influential low–Reynolds number simulations by Jiménez & Pinelli (1999) and Schoppa & Hussain (2002).

The focus on low Reynolds number is also often justified by the fact that the peak kinetic energy production occurs within the viscous buffer layer, at a wall-normal distance $y^+$ of approximately 12. It is important to note, however, that at high Reynolds numbers the major contribution to the bulk turbulence production comes from the logarithmic region. This is highlighted in **Figure 1*a***, which shows the production term with a logarithmic abscissa, as is traditionally done. This representation tends to obscure the contribution to the bulk production. **Figure 1*b*** instead shows the production in premultiplied form, where equal areas represent equal contributions to the total production. It is immediately clear that, whereas the main contribution to the bulk production comes from the near-wall region at low Reynolds numbers, the logarithmic region dominates at sufficiently high Reynolds numbers. The cross-over at which the contribution from the log region is equal to that from the near-wall region (taken nominally to be $y^+ \leq 30$) is estimated to occur at $Re_\tau \approx 4{,}200$.

A high–Reynolds number flow is defined by a sufficient separation of scales, but what is sufficient will depend on the flow under consideration and the purpose at hand. For wall turbulence, there are three primary length scales: the viscous length scale $\nu/u_\tau$, the Kolmogorov scale $\eta$, and the boundary-layer thickness $\delta$ (or equivalently the pipe radius or channel half-height). In the classical log-law description for the mean flow, one may define a high Reynolds number as one in which an appreciable length of logarithmic behavior is observed. This leads to a range of estimates depending

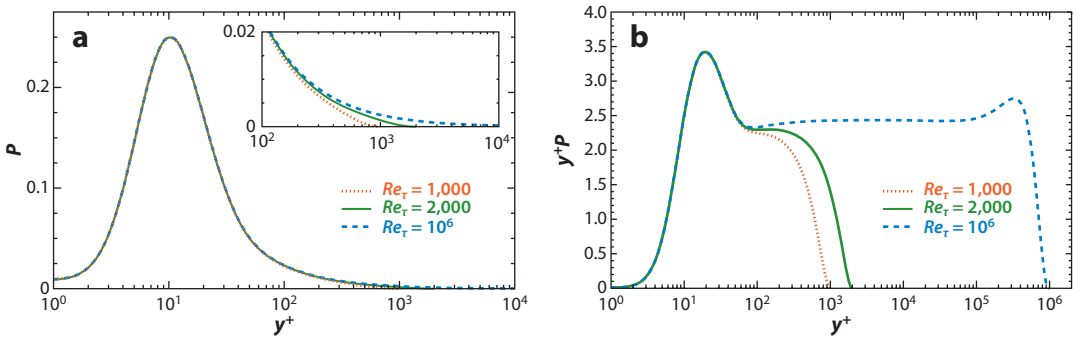


**Figure 1**

Turbulence kinetic energy production for a range of Reynolds numbers: (*a*) semi-logarithmic representation and (*b*) premultiplied representation (where equal areas represent equal contributions to the total production). The insert shows an expanded view of outer region. Here $P = -\overline{uv}^+ dU^+/dy^+$ is estimated using the law of wall-wake formulation for mean velocity for zero–pressure gradient boundary layers and the corresponding Reynolds shear stress profile as given by Perry et al. (2002). Figure taken from Marusic et al. (2010a). Reprinted with permission from Elsevier.



on where the log region is supposed to begin. It is clear now that the viscous influence on the mean velocity profile extends considerably further from the wall than previously understood. It had been commonly accepted that the effects of viscosity did not extend beyond $y^+ \approx 30$–$50$, but Zagarola & Smits (1998) found that for turbulent pipe flow, the profile followed a (Reynolds number–independent) power-law behavior for $60 < y^+ < 500$, and the profile did not begin to follow a logarithmic variation until $y^+ \geq 600$. A similar behavior has been observed for boundary layers, with a lower bound on the log law of approximately $y^+ = 200$ (Nagib et al. 2007, Sreenivasan & Sahay 1997). The important implication is that, to observe a logarithmic velocity variation in the velocity profile (e.g., a decade in $y^+$), the classical estimates of $30\nu/u_\tau < y < 0.15\delta$ require $Re_\tau > 2{,}000$, whereas those of Nagib et al. (2007) ($200\nu/u_\tau < y < 0.15\delta$) require $Re_\tau > 13{,}300$ and those of Zagarola & Smits (1998) ($600\nu/u_\tau < y < 0.12\delta$) require $Re_\tau > 50{,}000$.

Another criterion used in the past for so-called high–Reynolds number boundary layers is based on the momentum thickness. For example, Coles (1962) found that the wake factor $\Pi$ increased with Reynolds number to a maximum in the region of $Re_\theta = 6{,}000$ and then decreased until $Re_\theta \approx 15{,}000$, beyond which it appeared to attain a constant value slightly larger than 0.4. The maximum point corresponds to $Re_\tau \approx 2{,}400$, which is in line with having a logarithmic variation for $30\nu/u_\tau < y < 0.15\delta$. The comparable pipe Reynolds number for where the wake factor becomes constant is $Re_D = 400 \times 10^3$, in apparent agreement with the estimate by McKeon & Morrison (2007) for high–Reynolds number pipe flow.

All these estimates are based on the classical overlap of the inner and outer region and do not necessarily point to any specific changes that may occur in the coherent motions or the underlying physics as the Reynolds number increases. At any Reynolds number, the range of eddy scales found in wall turbulence is nominally from $12\eta$ to $30\delta$, where the smallest scale corresponds to the diameter of the filamentary (or worm-like) vortex structures (Stanislas et al. 2008), and the largest scale corresponds to the streamwise extent of the very-large-scale motions (VLSMs) that have been observed in pipes (Kim & Adrian 1999, Monty et al. 2009). It is instructive to consider this range of scales using spectra, as shown in **Figure 2** at $y^+ \approx 100$. Here, $k_x$ is the streamwise wave number. The $u$ spectra are premultiplied so that on this semilogarithmic plot the area under the curve for $k_x\phi_{uu}$ is $\overline{u^2}$, and the area under the curve for $k_x^3\phi_{uu}$ is proportional to an estimate for the dissipation rate. For $Re_\tau = 395$, little or no separation is seen between the energetic scales

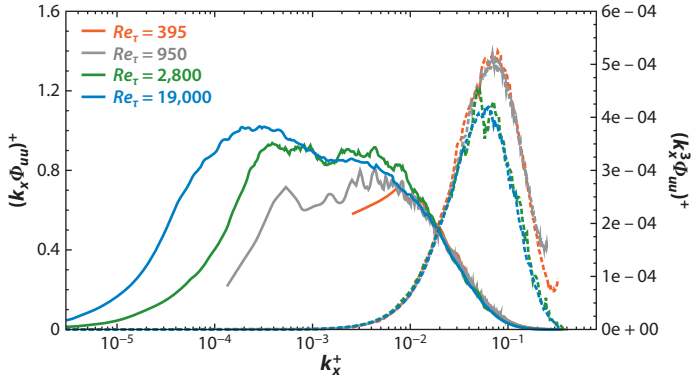


**Figure 2**

Streamwise $u$ spectra at $y^+ \approx 100$ from direct numerical simulations (DNS) of channel flow at $Re_\tau = 395$ (Moser et al. 1999) and 950 (del Álamo et al. 2004) and turbulent boundary layer experiments at $Re_\tau = 2{,}800$ and 19,000 (Mathis et al. 2009a). For all cases $\eta^+ \approx 2.8$. Here, the area under $k_x\phi_{uu}$ is $\overline{u^2}$, and the area under $k_x^3\phi_{uu}$ is proportional to an estimate of $\varepsilon$, the turbulent dissipation rate. The differences between the DNS and experimental $k_x^3\phi_{uu}$ curves likely result from the limited spatial resolution of the experimental data, as the expectation is that this part of the spectrum is independent of Reynolds number.



contributing to $\overline{u^2}$ and those contributing to the dissipation, and the separation emerges only slowly with increasing Reynolds number. Although the dissipation rate was estimated using the assumption of small-scale isotropy, which is known to underestimate the true dissipation rate, the conclusion remains the same. Along this line, McKeon & Morrison (2007) considered the scale separation necessary for the simultaneous appearance of a logarithmic layer in physical space and an inertial subrange in spectral space, indicative of a fully developed spectrum at small scales, or a decoupling of viscous and energetic scales. For this, they concluded that $Re_\tau > 5{,}000$ is required.

Another criterion for sufficiently high Reynolds number is found by considering the full $u$ spectrogram across the boundary layer, as done by Hutchins & Marusic (2007a,b). **Figure 3** shows two such plots at $Re_\tau = 1{,}010$ and 7,300. Here, Taylor's hypothesis is used so that $\lambda_x = 2\pi/k_x = 2\pi U/f$ (see the sidebar Taylor's Hypothesis). This representation clearly shows the evolution of two distinct (inner and outer) energy peaks in the premultiplied streamwise velocity spectra. Whereas the inner peak at ($y^+ = 15$; $\lambda_x^+ = 1{,}000$) is evident at both Reynolds numbers, the outer peak is barely distinguishable at the lower Reynolds number. This spectral peak separation starts to appear for $Re_\tau$ approximately greater than 1,700, but Hutchins & Marusic (2007b) proposed that $Re_\tau > 4{,}000$ is required to ensure a sufficient scale separation indicative of high–Reynolds number turbulence. This estimate is similar to that given by McKeon & Morrison (2007), and it is interesting that these arguments, addressing opposite ends of the scale range, yield a similar

## TAYLOR'S HYPOTHESIS

Taylor's frozen flow hypothesis allows temporal fluctuations to be interpreted as spatial fluctuations and establishes a duality between the frequency $f$ and wave number $k$. In essence, this requires that the turbulence is frozen or evolves on a timescale much larger than the advective one, such that the conversion from space to time can be made by using the local mean velocity as the convection velocity. The applicability of this hypothesis to wall-bounded flows is comprehensively discussed by del Álamo & Jiménez (2009) and Moin (2009).

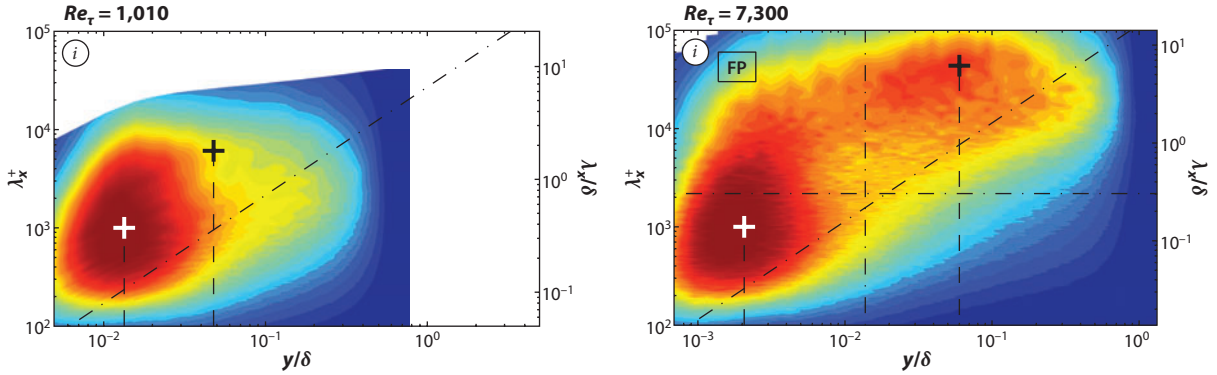


**Figure 3**

Contour maps showing the variation of one-dimensional premultiplied spectra with wall-normal position for two Reynolds numbers. An inner and an outer peak are noted at the higher Reynolds number. Figure taken from Hutchins & Marusic (2007a). Reprinted with permission from CUP.



estimate for a high Reynolds number. This similarity is supported by the observation that $\eta^+$ effectively scales universally as a function of $y^+$ in the inner region across a wide range of Reynolds numbers (Carlier & Stanislas 2005, Stanislas et al. 2008, Yakhot et al. 2010).

## 3. MEAN FLOW

As indicated above, the work of Barenblatt et al. (1997) stimulated a great deal of new work, especially with regard to the mean flow behavior. The Princeton Superpipe measurements (Zagarola & Smits 1998, McKeon et al. 2004) came under particular scrutiny, but a large number of new experiments in fully developed channel flows (Liu et al. 2001; Zanoun et al. 2003, 2009; Monty et al. 2007) and turbulent boundary layers (George & Castillo 1997, Österlund et al. 2000, Castillo & Johansson 2002, Chauhan & Nagib 2006, Nagib & Chauhan 2008, Nickels et al. 2007) were completed, over a reasonably large range of Reynolds numbers. To examine the very high–Reynolds number range, researchers also extensively investigated the neutral ABL, but the data are generally more useful for studies of turbulence rather than its mean velocity profile, with perhaps one exception (Andreas et al. 2006).

Several principal conclusions can now be made. First, the studies by George & Castillo (1997), Castillo & Johansson (2002), and George (2008) have highlighted the importance of the initial conditions on the development of turbulent boundary layers. Second, as discussed in Section 2, the viscous influence on the mean velocity profile extends considerably further from the wall than previously understood, and the lowest Reynolds number at which a logarithmic region is unambiguously present will depend on the flow, with substantial differences found between pipe flows and boundary layers. Third, there is now considerable evidence that the constants in the log law depend on the flow, so that the von Kármán constant for pipe flow, where McKeon et al. (2004) found $\kappa = 0.421$, is different from boundary-layer and channel flows, where Chauhan et al. (2007), Zanoun et al. (2003), and Monty (2005) found $0.384 < \kappa < 0.389$. Interestingly, the latter values agree well with the extensive data set obtained by Andreas et al. (2006) in the ABL over rough surfaces. These issues are discussed more fully by Marusic et al. (2010c), but it is clear that the classical view in which $\kappa$ was thought to be a universal constant has been brought into question (see the sidebar Log-Law Constants).

## LOG-LAW CONSTANTS

The accuracy of determining the constants in the log law depends on the Reynolds number, as at higher Reynolds number the region of logarithmic variation is larger, and on the accuracy to which we can measure the wall friction. For pipe and high-aspect-ratio channel flows, the wall friction can be determined with high accuracy from the pressure drop (typically <1% in $u_\tau$), but in boundary layers indirect methods need to be used, and consequently the accuracy of the wall friction measurements is generally not as good.



The choice of constants does not have a great impact on the shape of the profile, but the actual values sometimes make an appearance in turbulence models, for example, as in the model proposed by Spalart & Allmaras (1992), as well as in wall functions for Reynolds-averaged Navier-Stokes and large-eddy simulation methods, and therefore can have an important impact on, say, the prediction of vehicle drag [a difference of 6% in $\kappa$ can change the predicted skin friction coefficient by up to 2% at a length Reynolds number of $100 \times 10^6$, corresponding to that seen by a Boeing 747 fuselage in cruise (P.R. Spalart, private communication)].

In this respect, the computations of channel flows reported by Moser et al. (1999), del Álamo & Jiménez (2003, 2006), Abe et al. (2004), Hu et al. (2006), and Hoyas & Jiménez (2006) are not at a sufficiently high Reynolds number to make a supporting contribution. Jiménez & Moser (2007) have speculated that increasing the Reynolds number from the current maximum of 2,003 (Hoyas & Jiménez 2006) to 4,000 will allow a more definitive conclusion on the mean velocity scaling in the overlap region for high–Reynolds number channel flows. The corresponding bulk flow Reynolds number $Re_D$ is approximately $200 \times 10^3$, which agrees reasonably well with the value suggested by McKeon & Morrison (2007) for the transition to high–Reynolds number behavior in pipe flow, and the end of Blasius scaling for the friction factor in pipes and channels, which occurs at approximately $100 \times 10^3$ (McKeon et al. 2005, Yakhot et al. 2010). We will undoubtedly see the completion of such a massive computation in the not too distant future.

On the analytical side, a number of influential scaling arguments have been advanced, principally by Barenblatt et al. (1997), George & Castillo (1997), Wosnik et al. (2000), Monkewitz et al. (2007), Nagib et al. (2007), and Jones et al. (2008), with regard to the log-law/power-law debate (Marusic et al. 2010c). In addition to this, several extensions to the classical approach have been proposed, one notably by Wei et al. (2005), who argued, using the mean momentum equation, that the classical inner and outer layers need to be supplemented by intermediate layers. Such intermediate meso layers have been previously proposed (Sreenivasan 1989) and relate to the location of maximum Reynolds stress $y^+_{RSmax} \sim Re_\tau^{1/2}$. According to Klewicki et al. (2009), this results in the mean velocity profile approaching asymptotic logarithmic behavior only beyond $y^+$ approximately greater than $Re_\tau{}^{1/2}$. Here, $\kappa$ is seen as the output of a boundary value problem, and because different flows have different boundary conditions, it is expected that $\kappa$ would be different for different flows, as seen in recent experiments. Other extensions of the classic theory based on near asymptotics (Wosnik et al. 2000) and symmetry group methods (Oberlack 2001, Lindgren et al. 2004) result in a log law with a shifted origin, which is found to extend the fit to mean velocity data nearer to the wall (see also McKeon et al. 2005, Klewicki et al. 2009).

Resolving these issues will remain a challenge because of the slow trend toward asymptotic-like conditions, and a theoretical framework would seem essential. One promising framework is that of matched asymptotic expansions, as used by Monkewitz et al. (2008) in combination with composite profiles. The challenge here will be to develop a theoretical underpinning for the composite profiles that are used. Another approach is to consider more than just the mean

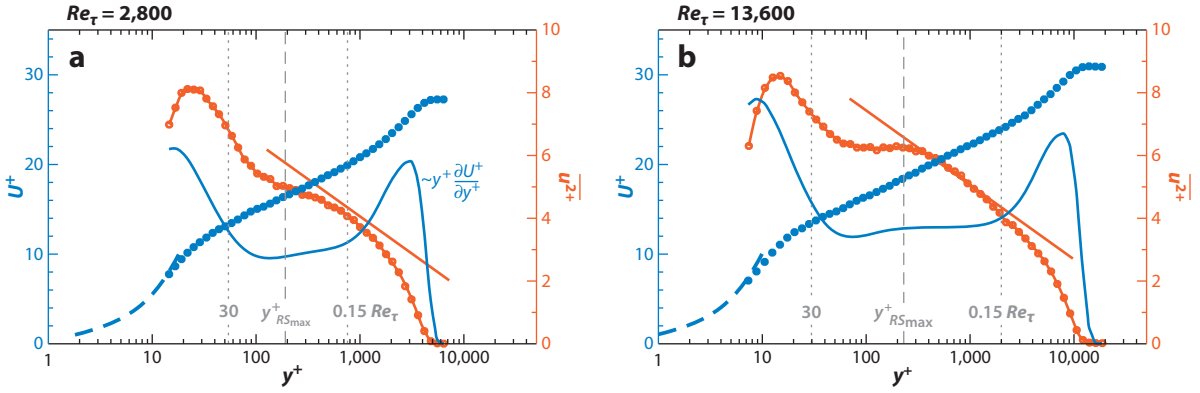


**Figure 4**

Mean velocity and streamwise turbulence intensity profiles for zero–pressure gradient boundary layers at $Re_\tau = 2{,}800$ (*a*) and 13,600 (*b*). Data taken from Hutchins et al. (2009). The solid blue line is the diagnostic function ($y^+\partial U^+/\partial y^+$) evaluated using a differencing scheme with a Savitsky-Golay filter. The solid orange line is the attached-eddy formulation [Equation 1 with $V(y^+) = 0$] as given by Perry & Li (1990). The location of the peak Reynolds shear stress is indicated by $y^+_{RS_{max}} = 2Re_\tau^{1/2}$.

velocity data. The Townsend-Perry attached-eddy model framework predicts that $\overline{u^2}$ (and $\overline{w^2}$) will also approach a logarithmic profile in the same region where the mean velocity is expected to be logarithmic (Townsend 1976), thus providing another diagnostic tool for quantifying this region (see Section 5). This is considered in **Figure 4** in which data for boundary layers are shown for two Reynolds numbers: $Re_\tau = 2{,}800$ and $Re_\tau = 13{,}600$. The function $y^+\partial U^+/\partial y^+$ is a constant in the region of logarithmic velocity variation, and it is often used as a diagnostic tool. On the basis of this diagnostic, the log region is yet to begin at the lower Reynolds number, but it is well-established at the higher value. From the figure, it is clear that determining the extent of the logarithmic layer from $U^+$ alone is difficult because of the slow departure from any log law, and the sensitivity of the diagnostic function ($y^+\partial U^+/\partial y^+$) to small measurement inaccuracies. The deviation from the logarithmic behavior for $\overline{u^2}$ in the near-wall region is more abrupt, thus making estimates for departures easier. Alternatively, measurements of $\overline{u^2}$ are not as accurate as for $U$, and this needs to be taken into account. Such behavior is consistent with the recent work of Eyink (2008), who proposed a modified attached-eddy approach to account for near-wall viscous effects, involving an $Re_\tau^{1/2}$ dependence consistent with the location of the peak Reynolds shear stress. It is interesting that the attached-eddy formulation of Marusic & Kunkel (2003) also involves a Reynolds number–dependent near-wall viscous contribution. The results in **Figure 4** do not resolve the issue of where the bounds of the logarithmic layer are, but this approach, which considers more than just the mean velocity, would seem valuable for future studies at higher Reynolds numbers.

## 4. ORGANIZED MOTIONS

In the current view of turbulent structure, we identify four principal characteristic elements. The first two, near-wall streaks with a typical spanwise spacing of approximately $100\nu/u_\tau$ (Kline et al. 1967) and hairpin or horseshoe vortices with a range of scales starting with a minimum height of $100\nu/u_\tau$ (Theodorsen 1952), have been recognized for a long time (see the sidebar Hairpin Vortices). More recently, visualizations, numerical studies, and experiments on wall flows have revealed the existence of two new elements, the so-called large-scale motions (LSMs) and VLSMs.

## HAIRPIN VORTICES

Theodorsen (1952) was the first to recognize the presence of loop-like vortical structures that originated at the wall and covered a range of scales. Although he proposed these horseshoe vortices to be the primary element of all turbulent shear flows, their importance and even their presence have long been debated (see, for example, Cantwell 1981). Head & Bandyopadhyay (1981) provided strong experimental evidence for their ubiquitous nature, but it was not until recently that computations by Wu & Moin (2009) corroborated their unambiguous and densely populated presence in boundary layers.



LSMs are believed to be created by the vortex packets formed when multiple hairpin structures travel at the same convective velocity (Kim & Adrian 1999, Zhou et al. 1999, Guala et al. 2006, Balakumar & Adrian 2007). They are related to the features seen by Head & Bandyopadhyay (1981) that consist of successive hairpins with their heads aligned along a line inclined at approximately 20° to the wall, and what has become clear, especially through the work of Adrian et al. (2000), is that these features are common and essential to the flow dynamics. A characteristic feature of LSMs is that the hairpin vortices within the packet align in the streamwise direction and induce regions of low-streamwise momentum between their legs (Brown & Thomas 1977, Adrian et al. 2000, Ganapathisubramani et al. 2003, Tomkins & Adrian 2003, Hutchins et al. 2005). LSMs have a streamwise scale of approximately 2–3$\delta$ and have been associated with the occurrence of bulges of turbulent fluid at the edge of the wall layer. A thorough review of the evidence supporting the existence of hairpin vortices and their organization into packets is provided by Adrian (2007).

Very long, meandering, features consisting of narrow regions of low-streamwise-momentum fluid flanked by regions of higher-momentum fluid have also been observed in the logarithmic and wake regions of wall flows (Kim & Adrian 1999, Tomkins & Adrian 2005, Guala et al. 2006, Balakumar & Adrian 2007, Hutchins & Marusic 2007b, Monty et al. 2007). In internal flows, the motions are typically referred to as VLSMs, whereas in external flows they are more commonly referred to as superstructures. Both VLSMs and superstructures appear to scale on outer variables, and although the spanwise/azimuthal meandering of these regions makes it difficult to determine their typical streamwise extent, hot-wire rake measurements in channels and pipes (Monty et al. 2007) have found instances of VLSM in internal flows as long as 30 times the channel half-height or pipe radius, whereas similar experiments in boundary layers (Hutchins & Marusic 2007b) show instances of superstructures with lengths up to 10–15 times the boundary-layer thickness. These lengths are typically shorter when inferred from single-point frequency spectra ($\sim$10–20$R$ for pipes and $\sim$6$\delta$ for boundary layers). In addition, Monty et al. (2009) noted that the superstructures in boundary layers appear to be limited to the logarithmic region, whereas for internal geometries the VLSMs are found to persist well into the outer layer (Bailey & Smits 2010). In contrast, Tutkun et al. (2009) found evidence of weak elongated structures within boundary layers out to the edge of the layer.

Spectral analysis of VLSM and LSM indicates that they make a significant contribution to the turbulent kinetic energy and Reynolds stress production (Guala et al. 2006, Balakumar & Adrian 2007), which distinguishes them from the inactive motions proposed by Townsend (1976). For example, Balakumar & Adrian (2007) found that 40%–65% of the kinetic energy and 30%–50% of the Reynolds shear stress are accounted for in the long modes with streamwise wavelengths $\lambda_x/\delta > 3$. Similar estimates for the contribution to the Reynolds shear stress from vortex packet structures were made by Ganapathisubramani et al. (2003), who used a feature-detection algorithm on stereoscopic particle image velocimetry (PIV) data in streamwise-spanwise planes in the log

layer. Careful analysis of DNS data has also revealed the footprint of the outer-scaled motions within the inner-scaled inner layer (Abe et al. 2004, Hoyas & Jiménez 2006, Hutchins & Marusic 2007a,b), and Mathis et al. (2009a) found modulation of the near-wall cycle by long-wavelength motions further from the wall, which is supported by the correlations measured by Tutkun et al. (2009) and the recent simulation results by Schlatter et al. (2009). These results suggest that motions in the logarithmic and outer layer may have a strong influence on the behavior of the near-wall turbulence.

The origin of the VLSMs and superstructures is not clear. Kim & Adrian (1999) proposed that the VLSMs are caused by pseudostreamwise alignment of the LSMs, whereas del Álamo & Jiménez (2006) suggested they could be formed by linear or nonlinear processes. Numerical experiments by Flores & Jiménez (2006) and Flores et al. (2007) in which the viscous wall was artificially removed, but the outer-flow structure remained essentially unchanged, suggest that the outer-layer dynamics are independent of the small near-wall structure. The measurements by Bailey & Smits (2010) in a pipe flow found that the VLSM peak in the autospectra is connected to structures with a large azimuthal scale, of approximately one-third of the circumference of the pipe. These structures also have large radial scales, which result in a strong correlation with motions near the wall, supporting the hypothesis that these structures are associated with the modulation of the near-wall flow observed by Hutchins & Marusic (2007b) and Mathis et al. (2009a,b).

The measurements by Bailey & Smits (2010) also suggest that in the outer layer (beyond the log region) the hairpin packets comprise detached eddies, which have little correlation with the flow near the wall and which occur across a wide range of azimuthal scales. Within the logarithmic region, it appears more likely that the hairpin packets are attached to the wall, and it is likely that it is these motions that modulate the near-wall cycle, as suggested by Mathis et al. (2009a). That is, we have two classes of LSM: near-wall attached LSMs and outer-layer detached LSMs. The similarity between the azimuthal scale of the detached LSMs in the outer layer and the VLSMs within the overlap layer suggests that if the VLSMs are caused by the streamwise alignment of the LSMs, only the LSMs in the outer layer are aligning to create these motions. Moreover, the detached LSMs appear to occur further from the wall than do the VLSMs and hence would be above them. In contrast, near the wall, the LSMs are attached to the wall, move at a different convection velocity, and have much smaller transverse scales than the VLSMs, and they are unlikely to be involved in the formation of VLSMs.

## 5. BEHAVIOR OF THE TURBULENT FLUCTUATIONS

Recent work has shed much light on how turbulence scales with Reynolds number. One notable achievement is a comprehensive description of the behavior of the variance of the streamwise turbulence $\overline{u^2}/u_\tau^2 = \overline{u^2}^+$ in boundary layers, as illustrated in **Figure 5**. The model proposed by Marusic & Kunkel (2003) builds on the attached-eddy model originally proposed for the logarithmic region of wall-bounded flows by Perry et al. (1986). Scaling arguments were advanced for particular regions of the spectrum, where low-wave-number motions were assumed to scale on outer-layer variables ($u_\tau$ and $\delta$), intermediate wave numbers were assumed to be related to attached eddies so that they scaled inversely with the distance from the wall ($y^{-1}$), and high wave numbers were assumed to follow Kolmogorov scaling. Overlap arguments then defined (for the logarithmic part of the velocity profile) a region of $k_x^{-1}$ and $k_x^{-5/3}$ in the $u$ spectrum. By integrating the spectrum, scaling laws were derived for smooth and rough walls (Perry & Li 1990). That is,

$$\overline{u^2}^+ = B_1 - A_1 \ln \frac{y}{\delta} - V\left(y^+\right), \tag{1}$$

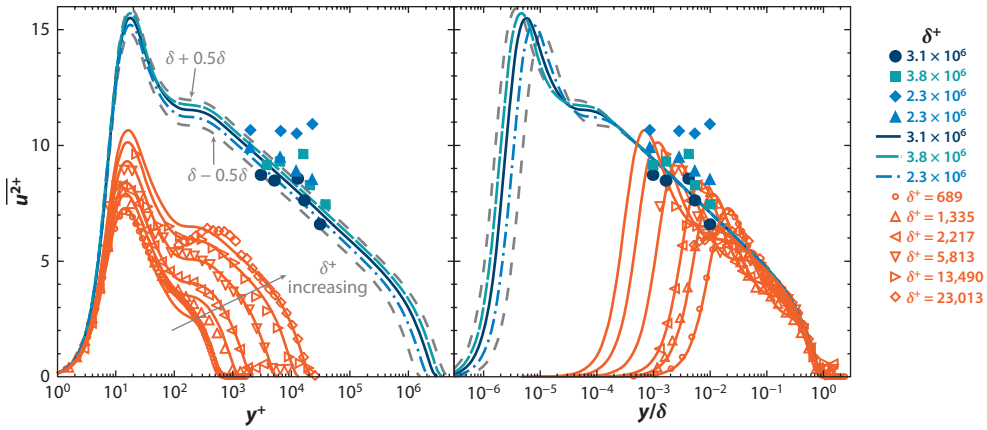


**Figure 5**

Streamwise turbulence intensity measurements in boundary layers. Filled symbols are atmospheric data, and open symbols are laboratory data. Solid, dashed, and dot-dashed lines are smooth-wall similarity formulations by Marusic & Kunkel (2003) that are also valid for rough walls in the outer region. Figure taken from Kunkel & Marusic (2006). Reprinted with permission from CUP.

where $B_1$ and $A_1$ are empirically derived constants (equal to 2.39 and 1.03, respectively), and the function $V(y^+)$ accounts for the integrated viscous contribution. By using largely empirical input, the model was later extended to cover the complete outer layer (Marusic et al. 1997), as well as the near-wall region (Marusic & Kunkel 2003). The success of this hybrid model is clear from the results shown in **Figure 5**.

The model also considered the behavior of $v$ and $w$. According to Townsend (1976), the $w$ component is expected to scale like $u$, in that the attached eddies will give rise to swirling motions in planes parallel to the wall that contribute to the turbulent kinetic energy but not the shear stress. The contribution to the shear stress is determined by $v$, which has a maximum near the heads of the attached eddies and is not expected to have a significant contribution from the large, outer-scaled motions. Hence, the $v$ spectra will show a scaling with $k_x^{-5/3}$ but not with $k_x^{-1}$. This is consistent with the $v$ spectra in the log region scaling with only $y$ and $u_\tau$ for all but the highest wave numbers, and this is strongly supported by the results shown in **Figure 6**, for data spanning a large range of Reynolds numbers.

Experimental data on $v$ and $w$ statistics at high Reynolds numbers are quite sparse, particularly in the near-wall region, primarily due to measurement difficulties in this region. Recent surveys of the available data by Jiménez & Hoyas (2008) and Buschmann et al. (2009), together with analysis of DNS data by del Álamo & Jiménez (2003), del Álamo et al. (2004), and Hoyas & Jiménez (2006), provide support for the Townsend attached-eddy hypothesis predictions for $v$ and $w$, but also highlight the differences between boundary layers and pipes and channels.

For the streamwise component, one obvious feature shown in **Figure 5** is the growth of the inner peak with Reynolds number, indicating a growing outer-layer influence on the near-wall motions. This growth assumes that the correct scaling is on $u_\tau$ and highlights the underlying inner-outer interactions (Hoyas & Jiménez 2006, Hutchins & Marusic 2007a). Alternative scalings have been proposed to explain these trends, most notably by DeGraaff & Eaton (2000), who proposed an empirical mixed scaling. However, Marusic & Kunkel (2003) showed that asymptotically a near-wall forcing based on the attached-eddy hypothesis leads to a form close to that of mixed scaling, and the success of the DeGraaff & Eaton (2000) scaling should not be interpreted as the outer motions scaling on $U_\infty$.

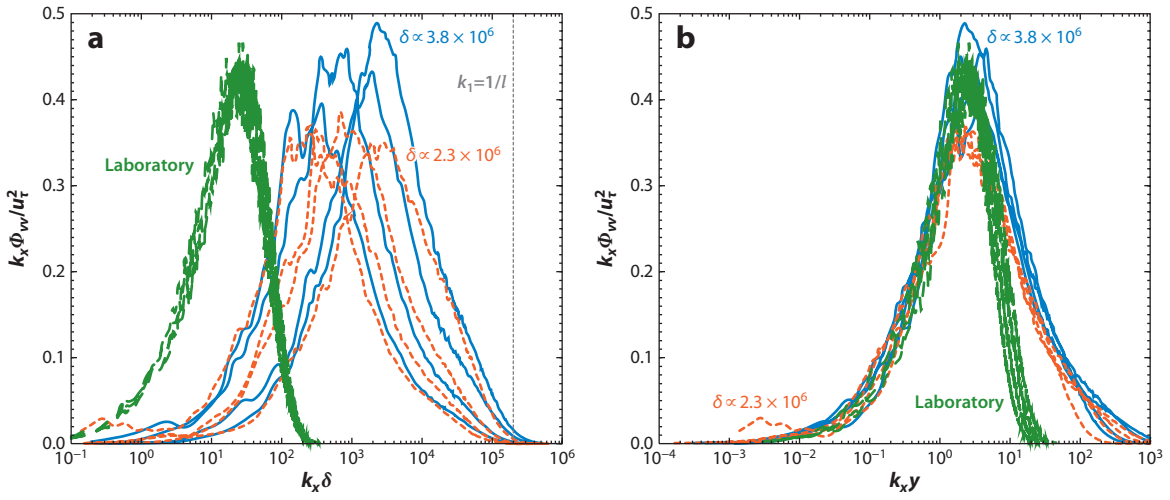


**Figure 6**

Spectra of the wall-normal component in the logarithmic region with (*a*) outer-flow scaling and (*b*) inner-flow scaling. Green lines are laboratory hot-wire data for $\delta^+ \propto 1 \times 10^3$. Other lines are from near-neutral atmosphere boundary-layer hot-wire measurements. Blue lines are for $\delta^+ \propto 3.8 \times 10^6$; orange lines are for $\delta^+ \propto 2.3 \times 10^6$ at $y/\delta = 0.00087$, 0.00305, 0.00522, and 0.01044, corresponding to $y^+ = 2{,}000$, 7,000, 12,000, and 24,000, respectively. Figure taken from Kunkel & Marusic (2006). Reprinted with permission from CUP.

The inner-outer interaction was considered by Hutchins et al. (2009) and Marusic et al. (2010a), who decomposed the velocity signatures across a boundary layer into small-scale ($\lambda_x < \delta$) and large-scale ($\lambda_x > \delta$) contributions using a simple cutoff spectral filter. **Figure 7*a*** indicates that the small-scale contribution is invariant with Reynolds number across most of the boundary layer, whereas the large-scale contribution clearly increases in magnitude at all wall-normal positions with increasing Reynolds number. The increasing influence due to the large-scale contributions in the near-wall region is noted. The result in **Figure 7** indicates that the $\overline{u^2}^+$ profile can be considered as the sum of two competing modes: a small viscous-scaled contribution primarily located in the near-wall region and a larger outer-scaled contribution peaking in the log region.

A question remains as to whether the behavior observed in boundary layers also occurs in other wall-bounded flows. Recent measurements in pipe flow in fact do not show an increase in the inner-layer peak in $\overline{u^2}^+$ with Reynolds number (Hultmark et al. 2010). This is part of the growing evidence demonstrating that pipe, channel, and boundary-layer flows behave differently in some substantial aspects. On the face of it, the invariance of the peak would indicate that there is no significant interaction between inner- and outer-layer motions in the near-wall region of a pipe. However, the underlying mechanisms may be more subtle. For example, the spectra for the pipe flow show a Reynolds number variation, whereas the variance (the integral of the spectra over all wave numbers) does not, so that the interactions among scales continue to evolve while the overall energy appears to be constrained by the fact that the flow is fully developed and there is no streamwise evolution of the global properties. Unfortunately, as Schlatter & Örlü (2010) demonstrated in a survey of seven investigations, DNS of boundary-layer flows for $Re_\tau$ up to 1,300 show surprisingly significant differences in basic integral quantities such as the friction coefficient $C_f$ or the shape factor $H$, and in their predictions of mean and fluctuation profiles, and they cannot be used solely to support any particular conclusion with regard to the inner peak behavior.

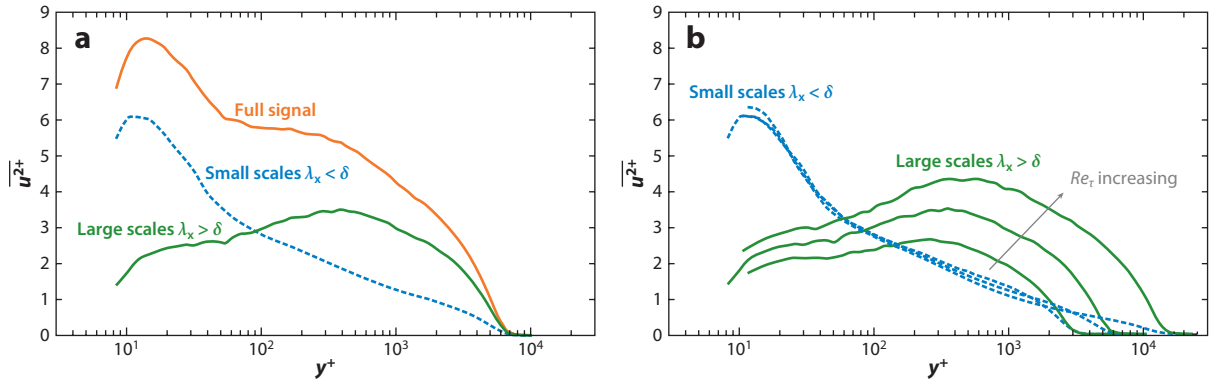


**Figure 7**

Scale decomposition of the streamwise turbulence intensity profile $\overline{u^2}/u_\tau^2$: (*a*) for $Re_\tau = 7{,}300$, together with the total (summed) contribution, and (*b*) for $Re_\tau = 3{,}900$, 7,300, and 19,000. Figure taken from Marusic et al. (2010a). Reprinted with permission from Elsevier.

One concept that continues to draw attention is the general notion of active and inactive motions. In Townsend's (1976) original proposal, the contribution of an attached eddy to the Reynolds shear stress is zero at the wall, reaches a maximum value near the eddy center, and then decreases further from the wall. Alternatively, its contribution to the intensities of components parallel to the wall remains finite at the wall (manifested as large-scale, swirling motions near the wall). The consequence is that superposition of the velocity fields of eddies with a wide range of scales, necessary to produce a uniform distribution of Reynolds stress, for example, will produce at the same time an inactive swirling motion near the wall with a magnitude that depends on the total thickness of the flow. This has been interpreted as a linear superposition, in that the inactive LSMs do not interact directly with the active Reynolds stress–bearing motions.

This description of the effects of attached eddies was later refined by Perry & Marusic (1995) with the introduction of type B (or wake) eddies in contrast to type A (or wall) eddies. The distinguishing feature of type B eddies is that they do not extend down toward the top of the viscous buffer zone, and whereas the type A eddies are responsible for a logarithmic velocity profile, the type B eddies are responsible for the wake region of the mean flow. [The attached and detached LSMs identified by Bailey & Smits (2010) may well be related to the type A and type B eddies.] Type B eddies do not produce an inactive component signature near the wall. However, the findings of Adrian et al. (2000) have shown that individual vortex structures are most often spatially aligned into streamwise packets, and these are more likely the representative attached-eddy structures (Marusic 2001) that lead to large-scale inactive signatures near the wall (while accounting for a significant proportion of Reynolds shear stress in the logarithmic region).

More recent studies have also shown that the large organized motions do more than just superimpose their signature on the near-wall region. For high–Reynolds number pipe flow, Morrison et al. (2004), Zhao & Smits (2007), and Morrison (2007) showed that the large eddies in the inner layer are not inactive, but rather they contribute to the energy production there, supporting Hunt & Morrison's (2001) suggestion, deduced from observations in the atmospheric surface layer, that at high Reynolds numbers, a top-down influence is dynamically significant, in addition to a bottom-up one that is likely to be more prevalent at low Reynolds numbers. Morrison et al. (2004) suggested that the large-scale contribution in the inner layer increases both as the Reynolds number increases and as distance from the wall decreases. Hutchins & Marusic (2007b) showed that

## TURBULENCE SPECTRUM

The full spectrum in wall turbulence is often divided into a number of ranges, including the low-wave-number energy-containing range in which the motions scale on the outer-layer variables such as $\delta$, the intermediate range in which the motions scale on the distance from the wall (the attached eddies), and the high-wave-number dissipation range in which the motions are comparable in size to the viscous or Kolmogorov length scale (see Perry et al. 1986). The subrange of wave numbers that overlaps the energy-containing and attached-eddy regions is expected to scale with $k_x^{-1}$, whereas the subrange that overlaps the attached eddy and dissipation regions is expected to scale with $k_x^{-5/3}$. In a log-log representation the slope of the spectrum is either $-1$ or $-5/3$. The $k_x^{-5/3}$ subrange is where the energy is transferred by inertial mechanisms from low to high wave numbers and is known as the inertial subrange.



the LSMs also modulate the near-wall processes, and this nonlinear interaction was quantified by Mathis et al. (2009a) using analysis tools based on Hilbert transforms and modeled mathematically as a predictive tool by Marusic et al. (2010b). The recent study by Schlatter et al. (2009) also shows evidence of this modulation process in DNS data.

The behavior of the spectra has also come under increased scrutiny. The scaling of turbulence logically proceeds from the spectral behavior, as typified by Perry & Chong's (1982) model, which in turn relies on the presence of robust scaling behaviors of the wave-number content, particularly the presence of $k_x^{-1}$ and $k_x^{-5/3}$ regions in the spectrum (see the sidebar Turbulence Spectrum). First, although the $k_x^{-5/3}$ region is well established, at least at high-enough Reynolds number, recent experiments indicate that the $k_x^{-1}$ region is only evident at very high Reynolds numbers over a very limited spatial extent (Nickels et al. 2005). Second, the interactions between inner- and outer-layer motions have become much clearer in recent years, and the simple division between inner- and outer-layer scaling that leads to the $k_x^{-1}$ region fails to capture those interactions. Specifically, the region where we might expect $k_x^{-1}$ scaling corresponds to the wave numbers occupied by the LSMs, and experiments have clearly shown that although the LSMs appear to behave as attached motions, they do not scale simply as $y^{-1}$. Third, the importance of the VLSMs was not appreciated until recently. For example, low-wave-number VLSMs contribute about half of the total energy content of the streamwise turbulence component (Balakumar & Adrian 2007). Fourth, it has become clear that the relative importance of LSMs, VLSMs, and superstructures depends on the nature of the flow: They behave differently in pipes, channels, and boundary layers (Monty et al. 2007, Bailey et al. 2008), something that is not captured in the attached-eddy model.

The issue of whether the superstructures found in boundary layers by Hutchins & Marusic (2007a) are the same as the VLSMs found in pipes by Kim & Adrian (1999) was investigated by Monty et al. (2009), who made detailed comparisons of the spectra in a pipe, channel, and zero–pressure gradient boundary layer with matched Reynolds number and measurement probe resolution. They concluded that, whereas the large-scale phenomena are qualitatively similar among the flows, the largest energetic scales in pipe and channels are distinctly different from those found in a boundary layer. They found that the contributions to the energy in internal flows continue to move to longer wavelengths with distance from the wall, whereas the opposite occurs in boundary layers, in which outer-flow structures shorten rapidly beyond the log region. Monty et al. (2009) noted that for $y/\delta < 0.5$ the different energy distributions in pipes and channels and zero–pressure gradient boundary layers occur in regions where the streamwise turbulence intensity is equal and from this concluded that all three flows might be of a similar type structure, with energy simply redistributed from shorter to longer scales for the pipe and channel flow cases. Whether the quantitative differences result from the interaction of the opposite wall in internal

flows or the intermittency of the outer region in boundary layers remains uncertain. One possible explanation put forward by Marusic & Adrian (2010) is that both superstructures in boundary layers and VLSMs in internal flows could be produced by concatenations of packets/LSMs but that this organization is distinctly different between the two types of flows. They noted that this may result from differences in the lateral organization or, in boundary layers, the interruption of wall-normal extent due to the entrained irrotational free-stream flow, which will limit the extent in the streamwise direction—akin to crystal growth limitations in materials due to grain boundaries.

The discussion of organized motions and eddy structure reaching far from the wall raises obvious and important questions concerning the appropriate convective velocity and coherence length. Renewed attention has been paid to the former issue in recent years, as direct comparisons between the spatial information generally obtained from simulation and temporal information from, for example, hot-wire experiments, converted to the spatial domain by the assumption of a suitable convective velocity distribution, have become possible. Mostly because of the lack of detailed information on more accurate expressions, the default assumption has been to use Taylor's (1938) hypothesis to convert between the domains. In practice, the energy associated with a particular scale is usually not localized in frequency and wave number, and correct conversion using Taylor's hypothesis requires identical distributions of energy in $\omega$ about a fixed $k_x$, and vice versa.

That this approximation fails, particularly at large scales and near the wall, has been known for some time (Wills 1964, Zaman & Hussain 1981). As the structure of higher–Reynolds number wall turbulence has been explored in more recent work, the details of the exact scale-dependent distribution of convective velocities have become more important. For example, the measurements of Metzger et al. (2007) in the atmospheric surface layer reveal temporal coherence at low frequencies over the first five meters, or $y^+ \sim 10^4$, which corresponds approximately to the upper edge of the log layer. In the range $O(10) < y^+ < O(10^4)$, the mean velocity increases by an order of magnitude, such that the same frequency may be identified as a superstructure far from the wall and something smaller than an LSM close to the wall.

The difficulties of obtaining simultaneous spatial and temporal information, particularly for higher Reynolds numbers, have meant that most studies of the convection velocity have been limited to low Reynolds number. Dennis & Nickels (2008) used time-resolved PIV in a turbulent boundary layer with $Re_\theta = 4{,}685$ to investigate the spatiotemporal ($k_x - \omega$) spectrum in a plane parallel to the wall at the outer edge of the log region. Their findings confirmed that the local mean velocity is a suitable velocity for conversion between the temporal and spatial domains at this location for all but the longest scales that could be resolved in their field of view, namely $6\delta$.

Closer to the wall, the differences between the temporal experimental streamwise spectra converted using Taylor's hypothesis and actual spatial spectra from the channel flow simulation by del Álamo et al. (2004) led Monty & Chong (2009) to propose a formulation for a wavelength-dependent convection velocity. This concept was extended by del Álamo & Jiménez (2009), whose formulation requires only local derivatives of the Fourier coefficients in time or space to obtain a distribution of convection velocities in ($k_x$, $k_z$, $\omega$) space (see also the commentary by Moin 2009). This is one of the few studies that address the appropriate convection velocity of all three velocity components, and the authors found them to be quite similar. A particularly notable observation is that above the logarithmic region, the large-scale contribution to the wall-parallel components convects with the local mean velocity, whereas the convection velocity of the contribution to the wall-normal component that has long spatial/temporal coherence corresponds to a point closer to the wall.

Another important conclusion arising from this study relates to the apparent stifling of any $k_x^{-1}$ region in the streamwise velocity spectrum by the increasing size of the range covered by the VLSMs in the frequency spectra as the Reynolds number increases. Del Álamo & Jiménez show

that the error associated with the use of Taylor's hypothesis at the large scales serves to push energy to the larger scales, leading to an erroneously large-energy amplitude at VLSM scales. It is worth noting, however, that Taylor's hypothesis must hold for the VLSMs somewhere in the wall-normal direction, where the convective velocity equals the local mean (which likely occurs in the log region, in the vicinity of the VLSM peak energy). Thus the full impact of the erroneous use of Taylor's hypothesis depends on the Reynolds number dependence of the location of this point and the true VLSM amplitude. McKeon (2008) and Mathis et al. (2009a) have shown that the location of this point moves closer to the wall with increasing Reynolds number, with the consequence that further investigation requires a focus on the very region of a high–Reynolds number flow that is most difficult to interrogate: an increasingly small near-wall region where spatial resolution issues become most insidious.

It should be noted that these approaches address the conversion between one-dimensional spatial and temporal spectra, or the convection velocity associated with the energy-weighted spectrum. Perhaps future studies will allow for a range of convection velocities at particular ($k_x$, $k_z$) scales.

## 6. DISCUSSION

The above sections clearly show that earlier modeling efforts did not account for the increasing energetic dominance and dynamic significance of the VLSMs with increasing Reynolds number. The relative magnitudes of $u$ and $v$ associated with very large scales are such that, although $v$ is small, the motions are clearly active in the sense of contributing to the Reynolds stress spectrum. There clearly also is a particular nonlinear interaction between the VLSMs and the smaller scales near the wall, which can be viewed either as an amplitude modulation effect or a preferred spatial phase relationship between the two, and it seems to provide an explanation for changing the sign of skewness in $u$ beyond the buffer region as the Reynolds number increases (Marusic et al. 2010b; Metzger & Klewicki 2001).

Conditional averaging techniques reveal that the signature of the very large scales takes a form resembling large streamwise roll cells, in agreement with the predictions of the most amplified structures from various linear theories (del Álamo & Jiménez 2006, McKeon & Sharma 2010). Although the origin of these very large scales has not been conclusively determined, they appear to be flow specific, as best exemplified by the direct comparison between streamwise spectra in pipes, channels, and boundary layers in Monty et al. (2009). A possible explanation for the origin of the very large scales has been given within the critical layer/forced system response framework of McKeon & Sharma (2010).

A question remains regarding the impact of the VLSMs and LSMs on the variation of the turbulence intensities, specifically $\overline{u^2}$. Although an increasing dominance of very large scales with a footprint at the wall would suggest that the near-wall peak value must increase with increasing Reynolds number, there appears to be contradictory evidence on this issue from different types of flow, as identified above. It is clear, however, that resolving this issue will require supplementary attention to experimental techniques, as ongoing work reports a surprising sensitivity of hot-wire results to both calibration and wire length (Hutchins et al. 2009, Hultmark et al. 2010, Marusic et al. 2010c). In the outer region, the collapse of the turbulent intensities normalized with the friction velocity shows a clear improvement with increasing Reynolds number, consistent with broader arguments about the nature of high–Reynolds number flows (McKeon & Morrison 2007, Yakhot et al. 2010).

These differences between low– and high–Reynolds number flows not withstanding, several important phenomena remain unchanged. Although the exact details of the mean velocity profile

remain in question, the classical structure of inner- and outer-layer overlap clearly is a robust first-order representation for pipes, channels, and boundary layers for all but the lowest Reynolds numbers. There is no conflict concerning the value of the von Kármán coefficient to the first decimal place at least! However, as technological advances have simultaneously extended the available Reynolds number range and reduced experimental error, some subtleties of the mean velocity scaling have emerged, along with the realization that we are still limited by the accuracy of the skin-friction measurement in turbulent boundary layers.

The turbulence structure near the wall, a principal part of modeling and control approaches, also appears to be a robust feature of turbulent flows. Results on the near-wall streak spacing, for example, have emphasized that this structure remains remarkably constant over a wide range of Reynolds numbers (Klewicki et al. 1995). In addition, inclined shear layers and associated correlation functions are observed at high Reynolds numbers that appear to be quite similar to those observed at lower Reynolds numbers (Hommema & Adrian 2003, Guala et al. 2006, Morris et al. 2007, Marusic & Hutchins 2008), and typical structure angles inferred from spatial correlations seem to be Reynolds number independent (Marusic & Heuer 2007). These results, together with predictions of the turbulence intensity variations, underscore the continued utility of attached-eddy concepts, as modified to include larger scales by Marusic (2001).

An overarching conclusion of this review is that the approach to an asymptotically high–Reynolds number state is slow, almost regardless of the diagnostic measure utilized. Hence there is a continued need for high–Reynolds number investigations. The challenge is to generate a large-scale separation while fully resolving all scales in space and time. One approach is to work with a facility for which the outer length scale is large. Experiments in the near-neutral atmospheric surface layer have been particularly useful in this regard, providing crucial evidence on Reynolds number trends (see, for example, Metzger & Klewicki 2001, Folz & Wallace 2009). These experiments are difficult, and it can be challenging to obtain accurate measurements, particularly with respect to a lack of control over the initial and boundary conditions. With these limitations in mind, the apparent robustness of the inferred trends to roughness, thermal, origin, and convergence effects, for example, is quite remarkable. In addition there are several larger laboratory-based facilities that will extend the flow regimes available to laboratory investigation, including the CICLOPE pipe (Talamelli et al. 2009) and the large wind tunnel under construction at the University of New Hampshire (J.C. Klewicki, private communication).

A second approach is to work with a facility for which the kinematic viscosity is small, such as in the Princeton Superpipe or the high–Reynolds number pressurized $SF_6$ wind tunnel under construction at the Max Planck Institute for Dynamics and Self-Organization (E. Bodenschatz, private communication). Measurement at increasingly small scales has been enabled by advances in micro- and nanofabrication techniques, from commercially available small hot-wire probes to the NanoScale Thermal Anemometry Probe developed at Princeton (Bailey et al. 2010). We note, however, that just as the spatial averaging implicit in near-wall Pitot probe measurements requires careful correction techniques, the accuracy of hot wires for predictive measurement in the near-wall region remains at the heart of several scaling questions, and therefore it is the subject of much current work (Marusic et al. 2010c).

Perhaps then future research will require hybrid techniques to ensure resolution of all scales [e.g., the combination of sonic anemometry and hot wires used by Kunkel & Marusic (2006) and Metzger et al. (2007), among others] and simultaneous spatial and temporal acquisition to address convection velocity concerns [e.g., the time-resolved PIV studies of Dennis & Nickels (2008)]. The numerical outlook suggests that even with the current rates of improvement of computing power, it will be a number of years before DNS can resolve a decade of self-similar scaling. However, the similarity of the small-scale near-wall structure and the increasing importance of the large

scales suggest that large-eddy simulation may have an important role to play in future advances in understanding. In this respect, large-eddy simulation of ABLs may prove to be particularly interesting, as it is always confronted with the physics of high–Reynolds number flows (e.g., see Khanna & Brasseur 1997, 1998; Bou-Zeid et al. 2005, 2008; Chung & Pullin 2009).

## DISCLOSURE STATEMENT

The authors are not aware of any affiliations, memberships, funding, or financial holdings that might be perceived as affecting the objectivity of this review.

## ACKNOWLEDGMENTS

This work was made possible by support received through NSF grant CTS-0625268, program manager William Schultz, and ONR grant N00014-09-1-0263, program manager Ronald Joslin (A.J.S.); AFOSR grant FA9550-09-1-0701, program manager John Schmisseur (B.J.M.); and the Australian Research Council (I.M.).

## LITERATURE CITED

Abe H, Kawamura H, Choi H. 2004. Very large-scale structures and their effects on the wall shear-stress fluctuations in a turbulent channel flow up to $Re_\tau = 640$. *J. Fluids Eng.* 126:835–43

Adrian RJ. 2007. Hairpin vortex organization in wall turbulence. *Phys. Fluids* 19:041301

**Adrian RJ, Meinhart CD, Tomkins CD. 2000. Vortex organization in the outer region of the turbulent boundary layer. *J. Fluid Mech.* 422:1–54**

Andreas EL, Claffey KJ, Jordan RE, Fairall CW, Guest PS, et al. 2006. Evaluations of the von Kármán constant in the atmospheric surface layer. *J. Fluid Mech.* 559:117–49

Bailey SSC, Kunkel GJ, Hultmark M, Vallikivi M, Hill J, et al. 2010. Turbulence measurements using a nanoscale thermal anemometry probe. *J. Fluid Mech.* In press

Bailey SCC, Hultmark M, Smits AJ, Schultz MP. 2008. Azimuthal structure of turbulence in high Reynolds number pipe flow. *J. Fluid Mech.* 615:121–38

Bailey SCC, Smits AJ. 2010. Experimental investigation of the structure of large- and very large-scale motions in turbulent pipe flow. *J. Fluid Mech.* 651:339–56

Balakumar BJ, Adrian RJ. 2007. Large- and very-large-scale motions in channel and boundary-layer flows. *Philos. Trans. R. Soc. Lond. A* 365:665–81

Barenblatt GI. 1993. Scaling laws for fully developed turbulent shear flows. Part 1. Basic hypotheses and analysis. *J. Fluid Mech.* 248:513–20

Barenblatt GI, Chorin AJ, Hald OH, Prostokishin VM. 1997. Structure of the zero-pressure-gradient turbulent boundary layer. *Proc. Natl. Acad. Sci. USA* 29:7817–19

Bou-Zeid E, Meneveau C, Parlange M. 2005. A scale-dependent Lagrangian dynamic model for large eddy simulation of complex turbulent flows. *Phys. Fluids* 17:025105

Bou-Zeid E, Vercauteren N, Parlange M, Meneveau C. 2008. Scale dependence of subgrid-scale model coefficients: an a priori study. *Phys. Fluids* 20:115106

Brown GL, Thomas ASW. 1977. Large structure in a turbulent boundary layer. *Phys. Fluids* 20:234–52

Buschmann M, Indinger T, Gad-el Hak M. 2009. Near-wall behavior of turbulent wall-bounded flows. *Int. J. Heat Fluid Flow* 30:993–1006

Cantwell BJ. 1981. Organized motion in turbulent flow. *Annu. Rev. Fluid Mech.* 13:457–515

Carlier J, Stanislas M. 2005. Experimental study of eddy structures in a turbulent boundary layer using particle image velocimetry. *J. Fluid Mech.* 535:143–88

Castillo L, Johansson TG. 2002. The effects of the upstream conditions on a low Reynolds number turbulent boundary layer with zero pressure gradient. *J. Turbul.* 3:31

**A comprehensive introduction to the existence of uniform momentum zones in turbulent boundary layers.**

Chauhan KA, Nagib HM. 2006. On the development of wall-bounded turbulent flows. In *IUTAM Symp. Comput. Phys. New Perspect. Turbul.*, ed. Y Kaneda, pp. 183–89. New York: Springer
Chauhan KA, Nagib HM, Monkewitz PA. 2007. Evidence of non-universality of Kármán constant. In *Progress in Turbulence 2. Proc. iTi Conf. Turbul.*, ed. M Oberlack, G Khujadze, S Guenther, T Weller, M Frewer, et al., pp. 159–64. New York: Springer
Chung D, Pullin DI. 2009. Large-eddy simulation and wall modelling of turbulent channel flow. *J. Fluid Mech.* 631:281–309
Coles DE. 1956. The law of the wake in the turbulent boundary layer. *J. Fluid Mech.* 1:191–226
Coles DE. 1962. The turbulent boundary layer in a compressible field. *Tech. Rep. R-403-PR, Append. A*, U.S. Air Force, Rand Corp.
**DeGraaff DB, Eaton JK. 2000. Reynolds-number scaling of the flat-plate turbulent boundary layer. *J. Fluid Mech.* 422:319–46**
del Álamo JC, Jiménez J. 2003. Spectra of the very large anisotropic scales in turbulent channels. *Phys. Fluids* 15(6):L41–44
del Álamo JC, Jiménez J. 2006. Linear energy amplification in turbulent channels. *J. Fluid Mech.* 559:205–13
del Álamo JC, Jiménez J. 2009. Estimation of turbulent convection velocities and corrections to Taylor's approximation. *J. Fluid Mech.* 640:5–26
**del Álamo JC, Jiménez J, Zandonade P, Moser RD. 2004. Scaling of the energy spectra of turbulent channels. *J. Fluid Mech.* 500:135–44**
Dennis DJC, Nickels TB. 2008. On the limitations of Taylor's hypothesis in constructing long structures in a turbulent boundary layer. *J. Fluid Mech.* 614:197–206
Donnelly RJ, Sreenivasan KR, eds. 1998. *Flow at Ultra-High Reynolds and Rayleigh Numbers*. Dordrecht: Kluwer
Eyink GL. 2008. Turbulent flow in pipes and channels as cross-stream "inverse cascades" of vorticity. *Phys. Fluids* 20:125101
Fernholz HH, Finley PJ. 1996. The incompressible zero-pressure-gradient turbulent boundary layer: an assessment of the data. *Prog. Aerosp. Sci.* 32:245–311
Fernholz HH, Krause E, Nockemann M, Schober M. 1995. Comparative measurements in the canonical boundary layer at $Re_\theta \leq 6 \times 10^4$ on the wall of the DNW. *Phys. Fluids* 7:1275–81
Flores O, Jiménez J. 2006. Effect of wall-boundary disturbances on turbulent channel flows. *J. Fluid Mech.* 566:357–76
Flores O, Jiménez J, del Álamo JC. 2007. Vorticity organization in the outer layer of turbulent channels with disturbed walls. *J. Fluid Mech.* 591:145–54
Folz A, Wallace JM. 2009. Near-surface turbulence in the atmospheric surface layer. *Physica D* 239:1305–17
Gad-el Hak M, Bandyopadhyay P. 1994. Reynolds number effects in wall-bounded turbulent flows. *Appl. Mech. Rev.* 47:307–65
Ganapathisubramani B, Longmire EK, Marusic I. 2003. Characteristics of vortex packets in turbulent boundary layers. *J. Fluid Mech.* 478:35–46
George WK. 2008. Is there an asymptotic effect of initial and upstream conditions on turbulence? *Proc. ASME 2008 Fluids Eng. Meet.*, Pap. FEDSM2008-55362
George WK, Castillo L. 1997. Zero-pressure-gradient turbulent boundary layer. *Appl. Mech. Rev.* 50:689–729
Guala M, Hommema SE, Adrian RJ. 2006. Large-scale and very-large-scale motions in turbulent pipe flow. *J. Fluid Mech.* 554:521–42
Head MR, Bandyopadhyay PR. 1981. New aspects of turbulent boundary-layer structure. *J. Fluid Mech.* 107:297–337
Hites MH. 1997. *Scaling of high-Reynolds number turbulent boundary layers in the National Diagnostic Facility*. PhD thesis, Ill. Inst. Technol.
Hommema SE, Adrian RJ. 2003. Packet structure of surface eddies in the atmospheric boundary layer. *Bound.-Layer Meteorol.* 106:147–70
Hoyas S, Jiménez J. 2006. Scaling of the velocity fluctuations in turbulent channels up to $Re_\tau = 2003$. *Phys. Fluids* 18:011702
Hu Z, Morley C, Sandman N. 2006. Wall pressure and shear stress spectra from direct simulations of channel flow. *AIAA J.* 44:1541–49

**Investigation of the Reynolds number scaling of the Reynolds stresses over a wide Reynolds number range and introduction of mixed scaling.**

**Scaling of velocity fluctuations in DNS of channel flow and implications for similarity in the outer scaling region.**

Hultmark MN, Bailey SCC, Smits AJ. 2010. Scaling of near-wall turbulence in pipe flow. *J. Fluid Mech.* 649:103–13

Hunt JCR, Morrison JF. 2001. Eddy structure in turbulent boundary layers. *Eur. J. Mech. B Fluids* 19:673–94

Hutchins N, Hambleton WT, Marusic I. 2005. Inclined cross-stream stereo particle image velocimetry measurements in turbulent boundary layers. *J. Fluid Mech.* 541:21–54

Hutchins N, Marusic I. 2007a. Evidence of very long meandering streamwise structures in the logarithmic region of turbulent boundary layers. *J. Fluid Mech.* 579:1–28

Hutchins N, Marusic I. 2007b. Large-scale influences in near-wall turbulence. *Philos. Trans. R. Soc. Lond. A* 365:647–64

Hutchins N, Nickels TB, Marusic I, Chong MS. 2009. Hot-wire spatial resolution issues in wall-bounded turbulence. *J. Fluid Mech.* 632:431–42

Jiménez J, Hoyas S. 2008. Turbulent fluctuations above the buffer layer of wall-bounded flows. *J. Fluid Mech.* 611:215–36

Jiménez J, Moser RD. 2007. What are we learning from simulating wall turbulence? *Philos. Trans. R. Soc. Lond. A* 365:715–32

Jiménez J, Pinelli A. 1999. The autonomous cycle of near-wall turbulence. *J. Fluid Mech.* 389:335–59

Jones MB, Nickels TB, Marusic I. 2008. On the asymptotic similarity of the zero pressure-gradient turbulent boundary layer. *J. Fluid Mech.* 616:195–203

Khanna S, Brasseur JG. 1997. Analysis of Monin-Obukhov similarity from large-eddy simulation. *J. Fluid Mech.* 345:251–86

Khanna S, Brasseur JG. 1998. Three-dimensional buoyancy- and shear-induced local structure of the atmospheric boundary layer. *J. Atmos. Sci.* 55:710–43

**Kim KC, Adrian RJ. 1999. Very large-scale motion in the outer layer. *Phys. Fluids* 11:417–22**

**Identification and discussion of the importance of the very large scales of motion in internal flows.**

**Kim J, Moin P, Moser RD. 1987. Turbulence statistics in fully developed channel flow at low Reynolds number. *J. Fluid Mech.* 177:133–66**

**Ground-breaking DNS of turbulent channel flow at $Re_\tau = 180$ and comparison of statistics with experimental data.**

Klewicki JC. 2010. Reynolds number dependence, scaling and dynamics of turbulent boundary layers. *J. Fluid Eng.* In press

Klewicki JC, Fife P, Wei T. 2009. On the logarithmic mean profile. *J. Fluid Mech.* 638:73–93

Klewicki JC, Metzger MM, Kelner E, Thurlow EM. 1995. Viscous sublayer flow visualizations at $R_\theta \approx 1{,}500{,}000$. *Phys. Fluids* 7:857–63

Kline SJ, Reynolds WC, Schraub FA, Rundstadler PW. 1967. The structure of turbulent boundary layers. *J. Fluid Mech.* 30:741–73

Kunkel GJ, Marusic I. 2006. Study of the near-wall-turbulent region of the high-Reynolds-number boundary layer using an atmospheric flow. *J. Fluid Mech.* 548:375–402

Lindgren B, Österlund JM, Johansson AV. 2004. Evaluation of scaling laws derived from Lie group symmetry methods in zero-pressure-gradient turbulent boundary layers. *J. Fluid Mech.* 502:127–52

Liu Z, Adrian RJ, Hanratty TJ. 2001. Large-scale modes of turbulent channel flow: transport and structure. *J. Fluid Mech.* 448:53–80

Marusic I. 2001. On the role of large-scale structures in wall turbulence. *Phys. Fluids* 13(3):735–43

Marusic I, Adrian RJ. 2010. The eddies and scales of wall turbulence. In *The Nature of Turbulence*, ed. PA Davidson, Y Kaneda, KR Sreenivasan. Cambridge, UK: Cambridge Univ. Press. In press

Marusic I, Heuer WD. 2007. Reynolds number invariance of the structure inclination angle in wall turbulence. *Phys. Rev. Lett.* 99:114504

Marusic I, Hutchins N. 2008. Study of the log-layer structure in wall turbulence over a very large range of Reynolds number. *Flow Turbul. Combust.* 81:115–30

Marusic I, Kunkel GJ. 2003. Streamwise turbulence intensity formulation for flat-plate boundary layers. *Phys. Fluids* 15:2461–64

Marusic I, Mathis R, Hutchins N. 2010a. High Reynolds number effects in wall turbulence. *Int. J. Heat Fluid Flow* 31:418–28

Marusic I, Mathis R, Hutchins N. 2010b. Predictive model for wall-bounded turbulent flow. *Science* 329:193–96

Marusic I, McKeon BJ, Monkewitz PA, Nagib HM, Smits AJ, Sreenivasan KR. 2010c. Wall-bounded turbulent flows: recent advances and key issues. *Phys. Fluids.* 22:065103

Marusic I, Uddin M, Perry AE. 1997. Similarity law for the streamwise turbulence intensity in zero-pressure-gradient turbulent boundary layers. *Phys. Fluids* 12:3718–26
Mathis R, Hutchins N, Marusic I. 2009a. Large-scale amplitude modulation of the small-scale structures in turbulent boundary layers. *J. Fluid Mech.* 628:311–37
Mathis R, Monty JP, Hutchins N, Marusic I. 2009b. Comparison of large-scale amplitude modulation in turbulent boundary layers, pipes, and channel flows. *Phys. Fluids* 21:111703
McKeon BJ, ed. 2007. Themed issue: scaling and structure in high Reynolds number wall-bounded flows. *Philos. Trans. R. Soc. A* 365(1852):633–876
McKeon BJ. 2008. *Scaling in wall turbulence: scale separation and interaction*. Presented at AIAA Theoret. Fluid Mech. Conf., 5th, Seattle, AIAA Pap. 2008-4237
McKeon BJ, Li J, Jiang W, Morrison JF, Smits AJ. 2004. Further observations on the mean velocity distribution in fully developed pipe flow. *J. Fluid Mech.* 501:135–47
McKeon BJ, Morrison JF. 2007. Asymptotic scaling in turbulent pipe flow. *Philos. Trans. R. Soc. Lond. A* 365:771–87
McKeon BJ, Sharma AS. 2010. A critical layer model for turbulent pipe flow. *J. Fluid Mech.* 658:336–82
McKeon BJ, Zagarola MV, Smits AJ. 2005. A new friction factor relationship for fully developed pipe flow. *J. Fluid Mech.* 538:429–43
Metzger MM. 2002. *Scalar dispersion in high Reynolds number turbulent boundary layers*. PhD thesis, Univ. Utah
**Metzger MM, Klewicki JC. 2001. A comparative study of near-wall turbulence in high and low Reynolds number boundary layers. *Phys. Fluids* 13:692–701**
Metzger MM, McKeon BJ, Holmes H. 2007. The near-neutral atmospheric surface layer: turbulence and non-stationarity. *Philos. Trans. R. Soc. Lond. A* 365:859–76
Moin P. 2009. Revisiting Taylor's hypothesis. *J. Fluid Mech.* 640:1–4
Monkewitz PA, Chauhan KA, Nagib HM. 2007. Self-contained high-Reynolds-number asymptotics for zero-pressure-gradient turbulent boundary layers. *Phys. Fluids* 19:115101
Monkewitz PA, Chauhan KA, Nagib HM. 2008. Comparison of mean flow similarity laws in zero pressure gradient turbulent boundary layers. *Phys. Fluids* 20:105102
Monty JP. 2005. *Developments in smooth wall turbulent duct flows*. PhD thesis, Univ. Melbourne
Monty JP, Chong MS. 2009. Turbulent channel flow: comparison of streamwise velocity data fom experiments and direct numerical simulation. *J. Fluid Mech.* 633:461–74
Monty JP, Hutchins N, Ng HCH, Marusic I, Chong MS. 2009. A comparison of turbulent pipe, channel and boundary layer flows. *J. Fluid Mech.* 632:431–42
Monty JP, Stewart JA, Williams RC, Chong MS. 2007. Large-scale features in turbulent pipe and channel flows. *J. Fluid Mech.* 589:147–56
Morris SC, Stolpa SR, Slaboch PE, Klewicki JC. 2007. Near surface particle image velocimetry measurements in a transitionally rough-wall atmospheric surface layer. *J. Fluid Mech.* 580:319–38
Morrison JF. 2007. The interaction between inner and outer regions of turbulent wall-bounded flow. *Philos. Trans. R. Soc. Lond. A* 365:683–98
Morrison JF, McKeon BJ, Jiang W, Smits AJ. 2004. Scaling of the streamwise velocity component in turbulent pipe flow. *J. Fluid Mech.* 508:99–131
Moser RD, Kim J, Mansour NN. 1999. Direct numerical simulation of turbulent channel flow up to $R_\tau = 590$. *Phys. Fluids* 11:943–45
**Nagib HM, Chauhan KA. 2008. Variations of von Kármán coefficient in canonical flows. *Phys. Fluids* 20:101518**
Nagib HM, Chauhan KA, Monkewitz PA. 2007. Approach to an asymptotic state for zero pressure gradient turbulent boundary layers. *Philos. Trans. R. Soc. Lond. A* 365:755–70
Nickels TB, Marusic I, Hafez SM, Chong MS. 2005. Evidence of the $k^{-1}$ law in a high-Reynolds-number turbulent boundary layer. *Phys. Rev. Lett.* 95:074501
Nickels TB, Marusic I, Hafez SM, Hutchins N, Chong MS. 2007. Some predictions of the attached eddy model for a high Reynolds number boundary layer. *Philos. Trans. R. Soc. Lond. A* 365:807–22
Oberlack M. 2001. A unified approach for symmetries in plane parallel turbulent shear flows. *J. Fluid Mech.* 427:299–328

**Investigation of the streamwise normal stress in the near-wall region over three decades of Reynolds number.**

**Development of a composite mean velocity profile shows that the von Kármán "constant" may in fact vary between canonical flows.**

Österlund JM. 1999. *Experimental studies of zero pressure-gradient turbulent boundary layer*. PhD thesis, KTH, Stockholm

Österlund JM, Johansson AV, Nagib HM, Hites MH. 2000. A note on the overlap region in turbulent boundary layers. *Phys. Fluids* 12:1–4

Panton R, ed. 1997. *Self-Sustaining Mechanisms of Wall Turbulence*. Southampton, UK: Comp. Mech. Publ.

Panton RL. 2001. Overview of the self-sustaining mechanisms of wall turbulence. *Prog. Aerosp. Sci.* 37:341–83

Panton RL. 2007. Composite asymptotic expansions and scaling wall turbulence. *Philos. Trans. R. Soc. Lond. A* 365:733–54

**Seminal description of the modern development of the attached-eddy hypothesis.**

**Perry AE, Chong MS. 1982. On the mechanism of wall turbulence. *J. Fluid Mech.* 119:173–217**

Perry AE, Henbest SM, Chong MS. 1986. A theoretical and experimental study of wall turbulence. *J. Fluid Mech.* 165:163–99

Perry AE, Li JD. 1990. Experimental support for the attached-eddy hypothesis in zero-pressure-gradient turbulent boundary layers. *J. Fluid Mech.* 218:405–38

Perry AE, Marusic I. 1995. A wall-wake model for the turbulence structure of boundary layers. Part 1. Extension of the attached eddy hypothesis. *J. Fluid Mech.* 298:361–88

Perry AE, Marusic I, Jones MB. 2002. On the streamwise evolution of turbulent boundary layers in arbitrary pressure gradients. *J. Fluid Mech.* 461:61–91

Robinson SK. 1991. Coherent motions in turbulent boundary layers. *Annu. Rev. Fluid Mech.* 23:601–39

Schlatter P, Li Q, Brethouwer G, Johansson AV, Hennningson DS. 2010. Simulations of spatially evolving turbulent boundary layers up to $Re_\theta = 4{,}300$. *Int. J. Heat Fluid Flow* 31(3):251–61

Schlatter P, Örlü R. 2010. Assessment of direct numerical simulation data of turbulent boundary layers. *J. Fluid Mech.* 659:116–26

Schlatter P, Örlü R, Li Q, Brethouwer G, Fransson JHM, et al. 2009. Turbulent boundary layers up to $Re_\theta = 2{,}500$ studied through simulation and experiment. *Phys. Fluids* 21:051702

**Linear-perturbation-based development of a mechanism for the origin of the near-wall cycle.**

**Schoppa W, Hussain F. 2002. Coherent structure generation in near-wall turbulence. *J. Fluid Mech.* 453:57–108**

Smits AJ, ed. 2004. *IUTAM Symposium on Reynolds Number Scaling in Turbulent Flow*. Dordrecht: Kluwer

Spalart PR. 1988. Direct simulation of a turbulent boundary layer up to $R_\theta = 1{,}410$. *J. Fluid Mech.* 187:61–98

Spalart PR, Allmaras SR. 1992. *A one-equation turbulence model for aerodynamic flows*. Presented at AIAA Aerosp. Sci. Meet. Exhib., 30th, Reno, AIAA Pap. 1992-0439

Sreenivasan KR. 1989. The turbulent boundary layer. In *Frontiers in Experimental Fluid Mechanics*, ed. M Gad el Hak, pp. 139–209. New York: Springer-Verlag

Sreenivasan KR, Sahay A. 1997. The persistence of viscous effects in the overlap region and the mean velocity in turbulent pipe and channel flows. See Panton 1997, pp. 253–71

Stanislas M, Perret L, Foucaut JM. 2008. Vortical structures in the turbulent boundary layer: a possible route to a universal representation. *J. Fluid Mech.* 602:327–82

Talamelli A, Persiani F, Fransson JHM, Alfredsson H, Johansson AV, et al. 2009. CICLoPE: a response to the need for high Reynolds number experiments. *Fluid Dyn. Res.* 41:021407

Taylor GI. 1938. The spectrum of turbulence. *Proc. R. Soc. Lond.* 164:476–90

Theodorsen T. 1952. Mechanism of turbulence. In *Proc. 2nd Midwest. Conf. Fluid Mech., Mar. 17–19*, pp. 1–19. Columbus: Ohio State Univ.

Tomkins CD, Adrian RJ. 2003. Spanwise structure and scale growth in turbulent boundary layers. *J. Fluid Mech.* 490:37–74

Tomkins CD, Adrian RJ. 2005. Energetic spanwise modes in the logarithmic layer of a turbulent boundary layer. *J. Fluid Mech.* 545:141–62

Townsend AA. 1976. *The Structure of Turbulent Shear Flow*. Cambridge: Cambridge Univ. Press

Tutkun M, George WK, Delville J, Stanislas M, Johansson PBV, et al. 2009. Two-point correlations in high Reynolds number flat plate turbulent boundary layers. *J. Turbul.* 10:1–23

Walker JDA, ed. 1991. *Turbulent Flow Structure Near Walls*. London: The Royal Society

Wei T, Fife P, Klewicki JC, McMurtry P. 2005. Properties of the mean momentum balance in turbulent boundary layer, pipe and channel flows. *J. Fluid Mech.* 522:303–27

Wills J. 1964. On convection velocities in turbulent shear flows. *J. Fluid Mech.* 20:417–32

**Wosnik M, Castillo L, George WK. 2000. A theory for turbulent pipe and channel flows. *J. Fluid Mech.* 421:115–45**

**Treatment of internal flows accounting for finite–Reynolds number effects and highlighting the mesolayer, a region always affected by viscosity.**

Wu X, Moin P. 2009. Direct numerical simulation of turbulence in a nominally-zero-pressure-gradient flat-plate boundary layer. *J. Fluid Mech.* 630:5–41

Yakhot V, Bailey SCC, Smits AJ. 2010. Scaling of global properties of turbulence and skin friction in pipe and channel flows. *J. Fluid Mech.* 653:65–73

Zagarola MV, Smits AJ. 1998. Mean-flow scaling of turbulent pipe flow. *J. Fluid Mech.* 373:33–79

Zaman KBMQ, Hussain AKMF. 1981. Taylor hypothesis and large-scale coherent structures. *J. Fluid Mech.* 112:379–96

Zanoun ES, Durst F, Nagib H. 2003. Evaluating the law of the wall in two-dimensional fully developed turbulent channel flows. *Phys. Fluids* 15:3079–89

Zanoun ES, Nagib HM, Durst F. 2009. Refined $C_f$ relation for turbulent channels and consequences for high *Re* experiments. *Fluid Dyn. Res.* 41:021405

Zhao R, Smits AJ. 2007. Scaling of the wall-normal turbulence component in high-Reynolds-number pipe flow. *J. Fluid Mech.* 576:457–73

Zhou J, Adrian RJ, Balachandar S, Kendall TM. 1999. Mechanisms for generating coherent packets of hairpin vortices in channel flows. *J. Fluid Mech.* 387:353–96

Annual Review of
Fluid Mechanics

Volume 43, 2011

# Contents

**Indexes**



**Errata**

An online log of corrections to *Annual Review of Fluid Mechanics* articles may be found at http://fluid.annualreviews.org/errata.shtml